Int. J. Hyperthermia, August 2011; 27(5): 491–502

informa
healthcare

RESEARCH ARTICLE

Nanoparticle distribution and temperature elevations in prostatic tumours in mice during magnetic nanoparticle hyperthermia

ANILCHANDRA ATTALURI[1], RONGHUI MA[1], YUN QIU[2], WEI LI[2], & LIANG ZHU[1]

[1]*Department of Mechanical Engineering, University of Maryland Baltimore County, Baltimore, MD and*
[2]*Department of Pharmacology and Experimental Therapeutics, University of Maryland, Baltimore, MD, USA*

(Received 18 January 2011; Revised 6 April 2011; Accepted 27 April 2011)

Abstract
Among a variety of hyperthermia methods, magnetic nanoparticle hyperthermia is a highly promising approach for its confined heating within the tumour. In this study we perform *in vivo* animal experiments on implanted prostatic tumours in mice to measure temperature distribution in the tumour during magnetic nanoparticle hyperthermia. Temperature elevations are induced by a commercially available ferrofluid injected via a single injection to the centre of the tumour, when the tumour is subject to an alternating magnetic field. Temperature mapping in the tumours during magnetic nanoparticle hyperthermia has demonstrated the feasibility of elevating tumour temperatures higher than 50°C using only 0.1 cm^3 ferrofluid injected in the tumour under a relatively low magnetic field (3 kA/m). Detailed 3-D nanoparticle concentration distribution is quantified using a high-resolution microCT imaging system. The calculated nanoparticle distribution volume based on the microCT scans is useful to analyse nanoparticle deposition in the tumours. Slower ferrofluid infusion rates result in smaller nanoparticle distribution volumes in the tumours. Nanoparticles are more confined in the vicinity of the injection site with slower infusion rates, causing higher temperature elevations in the tumours. The increase in the nanoparticle distribution volume in the tumour group after the heating from that in the tumour group without heating suggests possible nanoparticle re-distribution in the tumours during the heating.

Keywords: *infusion rate, magnetic nanoparticle hyperthermia, microCT, nanoparticle distribution, temperature, tumour*

Introduction

Chemo (drug/chemical) therapy, radiation, surgical ablation and hyperthermia methods are options generally available in cancer treatment. It is well known that chemotherapy has numerous side effects associated with the procedures. Radiation and surgical ablation can increase the survival rate in cancer patients but may not be efficient to completely eradicate irregularly shaped tumours [1, 2]. In the past three decades, hyperthermia has been investigated as an alternative to the traditional cancer treatments. It is preferable for patients diagnosed with unresectable or complicated tumours, or for patients who are looking for an alternative to costly and risky surgical procedures. Among a variety of hyperthermia methods, magnetic nanoparticle hyperthermia is a promising approach for its confined heating within the tumour [3, 4]. The efficacy of this method relies on the achieved tumour temperature elevations, which are largely determined by the nanoparticle concentration distribution in the tumour; therefore, having an imaging technique to directly visualise and analyse the three-dimensional nanoparticle distribution in tumours would greatly improve treatment protocols to kill all tumour cells while avoiding overheating in the surrounding healthy tissue.

Magnetic nanoparticles such as iron oxides magnetite Fe_3O_4 and maghaemite γ-Fe_2O_3 are biocompatible in human tissue [5] and can be delivered to

Correspondence: Liang Zhu, Ph.D., Associate Professor, Department of Mechanical Engineering, University of Maryland Baltimore County, 1000 Hilltop Circle, Baltimore, MD 21250, USA. Tel: 410-455-3332. Fax: 410-455-1052. E-mail: zliang@umbc.edu

ISSN 0265–6736 print/ISSN 1464–5157 online
DOI: 10.3109/02656736.2011.584856

tumours via systemic injections or intratumoural injections. The heat generated by nanoparticles when exposed to an external alternating magnetic field is mainly due to the Néel relaxation mechanism and/or Brownian motion of the particles [6, 7]. In the systemic injection, not all the nanoparticles injected into the blood stream may reach the target region and its distribution in tumours also may rely on the local blood perfusion rate and extent of vascular leakage, as well as the coating on the nanoparticles to enhance extravascular transport. The second approach, which is the focus of the current study, is to directly inject magnetic nanoparticles into the extracellular space in tumours. The advantage of intratumoural injection of nanoparticles is to confine the particles to the tumour region surrounding the injection site to achieve a desired thermal dosage in the tumour. Previous experimental studies [8–11] have shown that magnetic nanoparticle hyperthermia via intratumoural injections can be successfully used to treat prostate cancer. This approach has also been used to treat breast cancer, kidney tumours, and liver cancer [12–14]. A previous *in vivo* animal study on rat muscle tissue has suggested an injection amount of 0.2 cm^3 of magnetic nanofluid (3.8% nanoparticle concentration) to achieve at least 6°C temperature elevations under a magnetic field of only 2 kA/m [16]. Another advantage of intratumoural injections is the ability to design optimised treatment protocols using multiple injection sites to generate sufficient temperature elevations for the entire tumour. A computer algorithm developed by Salloum et al. [17] has identified an injection strategy to achieve the isotherm of 43°C almost on the boundary of an irregularly shaped tumour. The developed algorithm allows adjustments of injection parameters such as injection rate and injection amount to elevate at least 90% of a tumour above certain threshold temperature (43°C), while less than 10% of the normal tissue temperatures exceed this threshold, when one designs a treatment protocol for an irregularly shaped tumour. As suggested by the previous results, it is important to understand how the injection parameters affect the heat generation pattern in real tumours for designing optimal protocols using the computer algorithm.

Previous experiments have shown the feasibility to investigate nanoparticle distribution using semi-transparent agarose gels [15, 18]. Since ferrofluid appears black in the semi-transparent gel, a photo image of the gel provides the general geometrical shape of the ferrofluid spreading after injection. It has been shown that the nanoparticles were confined to the vicinity of the injection site and particle deposition was greatly affected by the injection rate and amount [15, 16, 18]. Although the tissue equivalent gels cannot completely mimic the real biological tissue, those gel studies have demonstrated that implementing a very slow injection rate (~5 μl/min) is critical to have controlled and repeatable nanoparticle concentration distributions. Detailed nanoparticle deposition in the gel is difficult to quantify only based on the photo image of the gel. The local nanoparticle distribution has been quantified via direct measurement of the specific absorption rate (SAR) values at individual gel locations via $SAR = \rho C_p \frac{\partial T}{\partial t}\big|_{t=0}$, where ρ is density, C_p is specific heat, T is temperature and t is time. This method is based on the assumption of negligible heat conduction in the tissue before the heating is turned on. It has been shown from previous studies [15, 18] that the nanoparticle concentration is not uniform in the gel. Understanding nanoparticle distribution in real tissue is even more difficult to quantify since tissue is opaque. Typically, an assumed SAR distribution is proposed and the unknown parameters in the SAR expression are adjusted to have the best agreement between experimentally measured temperature elevations in tissue and theoretically predicted temperature field based on the proposed SAR expression [16]. The accuracy of this approach depends on the certainty of the temperature sensor locations in the tissue and how well the theoretical simulation models the actual tissue geometry and vasculature.

Nanostructures used in hyperthermia cancer treatment have a similar size range as the hydrodynamic radius of macromolecules in previous drug delivery studies. Some of the previous animal studies of large molecular drug transport in cancer treatment may be applicable to the transport properties of nanostructures in tumours. Typical experimental approaches of evaluating drug/nanostructure distribution in tumours utilise fluorescently labelled drug molecules in implanted tumours. Due to the penetration limitation of confocal microscopy (up to 200 μm in depth) and other optical methods, drug transport in the interstitial space in tumours is evaluated via a 2-D cranial or dorsal window chamber tumour preparation [19–21]. The complicated heterogeneous 3-D tumour structure may not be well represented in those 2-D tumour preparations, and 3-D transport process is often not realistically captured by those approaches.

X-ray computed tomography (CT) nowadays is a well-established standard diagnostic tool in medical fields for inspection and testing. MicroCT offers a non-destructive way to obtain complete high resolution three-dimensional spatial morphology of small specimen (up to 6 cm in dimension). Recently, iron-based nanoparticles have gained prominence in medical imaging [14, 22, 23]. Several previous works [10, 11, 14] have shown that CT can be used to guide the intratumoural injection of ferrofluid. However, those studies are limited by their

spatial resolution in the CT images (~1 mm) with only a few temperature measurements in tissue. Recent research by our group has shown the feasibility of using a high-resolution microCT imaging system to quantify not only detailed nanoparticle concentration distribution in agarose gels but also the linear correlation between the local nanoparticle concentration and its generated SAR value [18]. Although the microCT does not allow direct visualisation of individual nanoparticles, the accumulation of nanoparticles in the gel results in a region with a much higher density than the rest of the gel area and the density variation is detected by the microCT system. Agarose gel is a biphasic viscoelastic solid. Its shear modulus is negligible compared to its bulk modulus. Gel acts like rubber materials under application of internal pressure, which leads to swelling. Unlike real tissue, which can sustain sufficiently high pressure elevation without breakage, gel typically has a very low tolerance to local pressure rises. The low pressure tolerance by gel makes it unsuitable to apply the gel results to actual tissue, including tumours. In addition, gel cannot mimic the actual blood perfusion in real tissue; therefore, the measured temperature elevations in gel are not applicable to realistic thermal conditions associated with *in vivo* animal studies or clinical trials. It is critical to use a three-dimensional imaging technique to understand how the injection parameters affect the actual nanoparticle concentration distribution in tumours and to investigate the correlation between achieved tumour temperature elevations and nanoparticle distribution.

In this study we perform *in vivo* animal experiments on implanted prostatic tumours in mice to measure temperature elevation distribution in the tumour during magnetic nanoparticle hyperthermia. Temperature rises are induced by a commercially available ferrofluid injected to the centre of the tumour, when the tumour is subject to an alternating magnetic field. The tumours resected from the mice before and after the heating experiment are scanned in a high-resolution microCT imaging system. The effects of the ferrofluid infusion rate on the nanoparticle distribution and the obtained temperature elevation distribution in the tumours are evaluated in the study. A possible nanoparticle redistribution after heating will be discussed.

Experimental methods and materials

Animals and tumour models

Fifteen Balbc/c Nu/Nu male mice [mean ± SD: 25.44 ± 5.51 g] bearing PC3 xenograft tumour were used for this study. The mice were purchased from the National Cancer Institute. Each mouse was inoculated on both flanks with 10^7 PC3 human prostate cancer cells via a sterile 26-gauge needle injection at the University of Maryland, Baltimore (UM,B). Once the tumours reached a diameter of 10 mm, the mice were brought to the laboratory at the University of Maryland Baltimore County (UMBC) for the nanoparticle hyperthermia experiment. Depending on individual mice, it usually took 6–8 weeks for the tumour to reach the desired size measured by a calliper. The mouse was anaesthetised with sodium pentobarbital solution (40 mg/kg, i.p.), and placed on a water-jacketed heating pad to maintain a normal body core temperature monitored by a thermocouple inserted into the rectum. The detailed animal protocol has been approved by both UM,B and UMBC Institutional Animal Care and Use Committees (IACUCs).

Nanoparticle injections

Water-based ferrofluids (EMG705 series, Ferrotec, Nashua, NH) with a concentration of 5.8% by volume and a particle size of 10 nm were used in this study. The ferrofluid was loaded on a syringe pump (Genie Plus, Kent Scientific, Torrington, CT) to control the infusion flow rate and the amount of the injection. A 26-gauge Hamilton needle (Fischer Scientific, Springfield, NJ) was used for injecting ferrofluid into one of the two tumours (Figure 1). An injection amount of 0.1 cm^3 was adequate to elevate temperatures to at least 50°C, which is sufficiently high to kill tumour cells when the heating duration is longer than 15 min; therefore the injection amount was selected as 0.1 cm^3. Based on the density of magnetite (5240 kg/m^3) and the given ferrofluid concentration, each 0.1 cm^3 of ferrofluid contained approximately 25.2 mg of iron.

In this study, we wanted to evaluate how the infusion flow rates affect the nanoparticle distribution and temperature elevations in the tumour. Three mouse groups were included in the study, and individual groups represented different infusion flow rates, including 5 μL/min, 10 μL/min, and 20 μL/min [15, 16, 18]. For each infusion flow rate, five tumours were used to analyse the data. Mice were randomly placed into different experimental groups.

Magnetic field and temperature measurements

After the ferrofluid injection, two thermocouples (T-type, copper-constantan wires, 50 μm diameter) were inserted into the tumour to map the steady-state temperature elevations in the tumour. A gauge 22 needle was inserted in the tumour and it passed through the tumour centre all the way to the other side of the tumour. The thermocouple was inserted into the needle from one side of the tumour until it reached the opposite side. The needle was then

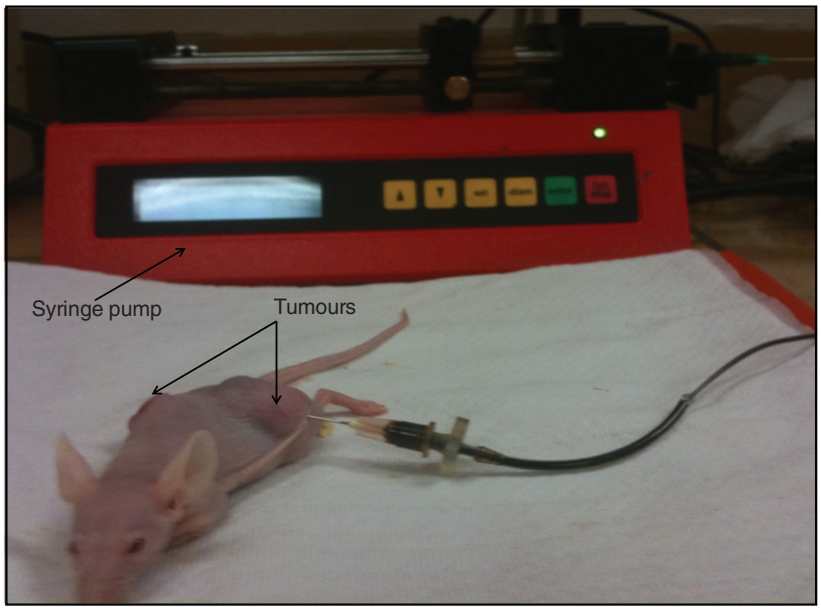

Figure 1. Ferrofluid injection into one of two tumours implanted in a mouse.

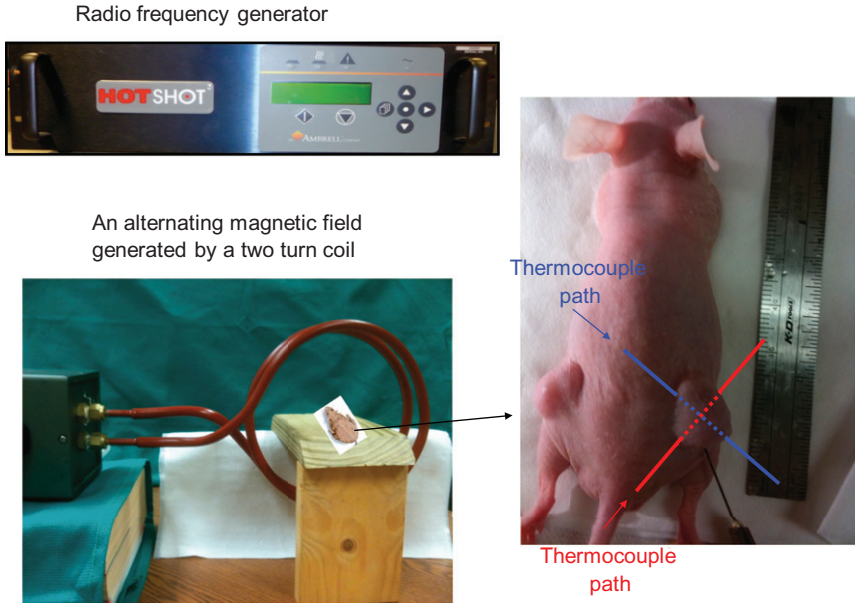

Figure 2. Experimental setup for the animal study including the radio frequency generator, a two turn coil for generating an alternating magnetic field, a stage for placing the mouse. The image on the right shows the tumours implanted in the mouse, the needle for injecting the ferrofluid, and two thermocouple paths to map the tumour temperature distribution.

withdrawn and removed since the metal needle can be heated in the presence of the magnetic field. Another thermocouple was inserted similarly except that the needle paths were perpendicular to each other, shown in Figure 2. Three more thermocouples were used to monitor the rectum, skin and environment temperatures. A radio-frequency generator (Hotshot 2, Ameritherm, Rochester, NY) was used to induce an alternating current of 400 A at a frequency of 190 kHz. The current passes through a custom-made two-turn water-cooled coil of 15 cm in diameter to generate a magnetic field inside the coil (Figure 2). The mouse was placed on a custom-made stage inside the coil such that the centre of the tumour with the nanoparticle injection is located at the coil centre where the magnetic field strength reached its maximum value (3 kA/m). Since the magnetic field distribution was axi-symmetric inside

the coil and the tumour was relatively small, the variation of the magnetic field inside the whole tumour can be considered negligible.

Our preliminary studies have shown that it takes less than 15 min to establish a steady state using the alternating magnetic field in this study. After a steady state was established, the temperature measurements along both tumour tissue paths were performed when one withdrew the thermocouples from their initial positions at an increment of 2 mm until they reached the other end of the tumour tissue path (see Figure 2). The thermocouple stayed at each tissue location for 20 s. This time duration is considered much longer than the characteristic time for the thermocouple to approach the same temperature as the tissue. Temperatures were recorded using a LabView® program running on a personal computer.

After the heating experiment, the mouse was removed from the stage. Whenever possible, the other tumour, located contra-laterally in the mouse, was used to evaluate the nanoparticle distribution without heating. The same amount of ferrofluid was injected into the contra-lateral tumour using the same infusion flow rate after the heating experiment for microCT imaging analyses. Then the mouse was euthanised with sodium pentobarbital overdose (160 mg/kg, i.p.). Both tumours were removed for the microCT scan.

MicroCT imaging and image analyses

Each tumour was placed in a microCT imaging system for scanning immediately after the *in vivo* experiment. A high-resolution microCT imaging system (Skyscan 1172, Microphotonics, PA) was used to image the nanoparticle distribution in the tumour tissue. The tumour was placed in low-density Styrofoam, and mounted on the platform of the imaging system with the help of a stage holder. A medium resolution scan of 17 μm (pixel size) was selected at 100 kV and 100 μA without a filter. The total CT scan time was typically less than 20 min. The images acquired from the microCT scan were then reconstructed using the NRecon® software package provided by Microphotonics. Scan parameters and reconstruction parameters were kept the same for all the scanned tumours in the study. The reconstructed images were analysed using the CTan® software package. In the scanned images and reconstructed image, the brightness is represented by the pixel index numbers between 0 and 255.

The total region of interest (ROI) was selected by interpolating the local ROI (ROI of each individual slice) throughout the selected tissue region. This procedure helped estimate the tumour boundaries and its volume (mean ± SD: $2.57 \pm 1.26\,cm^3$) and also minimised the total memory. The pixel index number for the tumour tissue ranged from 45 to 50, based on scanning results of tumours without ferrofluid injections. Adding nanoparticles in tumours increased the local pixel density and result in a larger pixel index number, and the region occupied by nanoparticles appeared brighter in the images. In this study, we assumed that a pixel region having a pixel index number higher than 55 contained nanoparticles. Pixel index numbers between 55 and 60 indicated pixels with low particle concentrations. The calculated nanoparticle distribution volume for the range of 55–60 represents regions with low nanoparticle concentration. By comparing the calculated distribution volumes related to different nanoparticle concentrations, one can draw conclusions whether nanoparticles are uniformly distributed or not in the tumour. Hence, the calculated nanoparticle distribution volume associated with various pixel index number ranges could be used to estimate how different nanoparticle concentrations were distributed in the tumour.

Using the CTan® software the highest density voxels along lines projected through the volume data set were selected and then incorporated into a two-dimensional image. By stacking all the two-dimensional images together, a pseudo three-dimensional projection of the inner nanoparticle distribution could be visualised. This technique is known as maximum intensity projection (MIP). MIPs of the scanned tumour with nanoparticles were acquired and used to quantitatively compare the nanoparticle distribution patterns affected by various factors.

Statistical analysis

The nanoparticle distribution volume and temperatures at all positions and other parameters of all three experimental groups were analysed and expressed as mean ± SD. Differences among the mean values of temperatures or nanoparticle distribution volume were determined by one-way repeated measures ANOVA. The post hoc comparisons between any two infusion rate groups were performed by the Student's t-test. Significance was evaluated at the 5% confidence level.

Results

Temperature distribution

Typical temperature distributions along the tumour tissue paths obtained during the magnetic nanoparticle hyperthermia treatment are shown in Figure 3. Both curves represent the steady-state tumour temperatures measured by the two thermocouples along

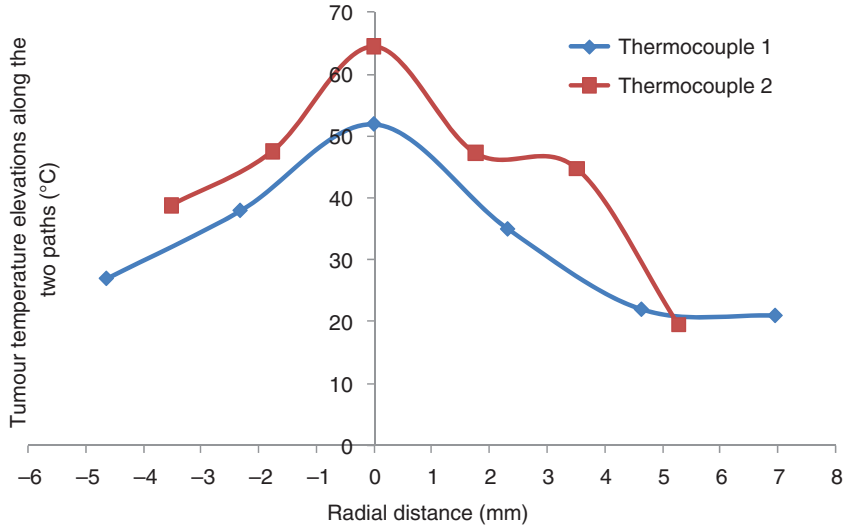

Figure 3. Typical temperature elevation profile in a tumour after steady state. The ferrofluid was injected at the 5 μL/min infusion rate.

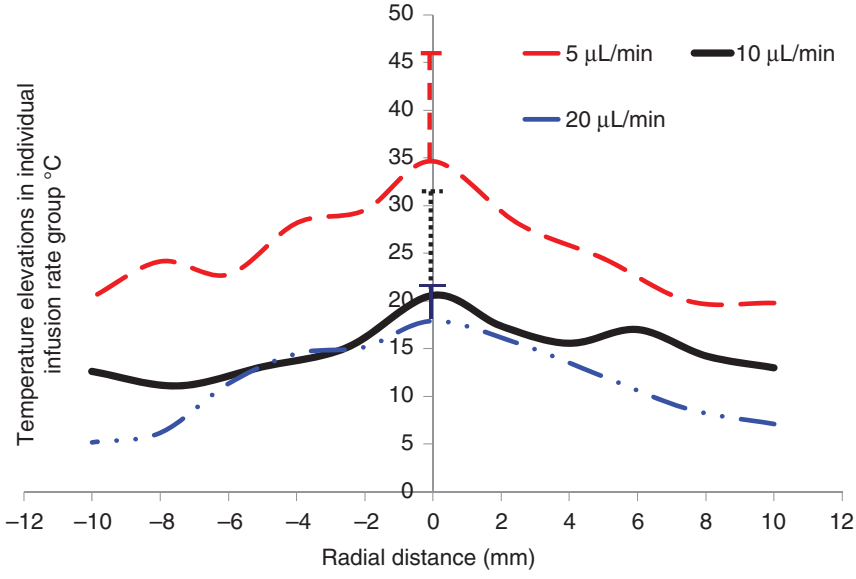

Figure 4. Tumour temperature distributions affected by different ferrofluid infusion rates.

the tumour paths. Although we have tried our best to have both paths passing through the tumour centre, it may not occur for this tumour. The maximum temperature is close to the injection site (tumour centre) and significant temperature elevations are observed. A bell like distribution of the temperature profile as a function of radial distance from the injection site can be seen in Figure 3. For a typical tumour of 10 mm in diameter, the minimal temperature elevations occur at the tumour boundary surface and they are still larger than 20°C, above the baseline temperature of approximately 37°C.

The temperature elevations measured in all the tumours are grouped together to evaluate the effect of the ferrofluid infusion flow rate on the temperature elevations. Figure 4 shows the variation of temperature profile as a function of the distance from the injection site for different infusion flow rates. Temperature elevations from all the trials for a specific infusion flow rate is set as a function of the distance from the injection site and a best-fit curve is used to fit the data. To achieve a minimal temperature elevation of 10°C for 20 min [24] in the entire region of a tumour used in this study, the infusion rate should be lower than 10 μL/min. The

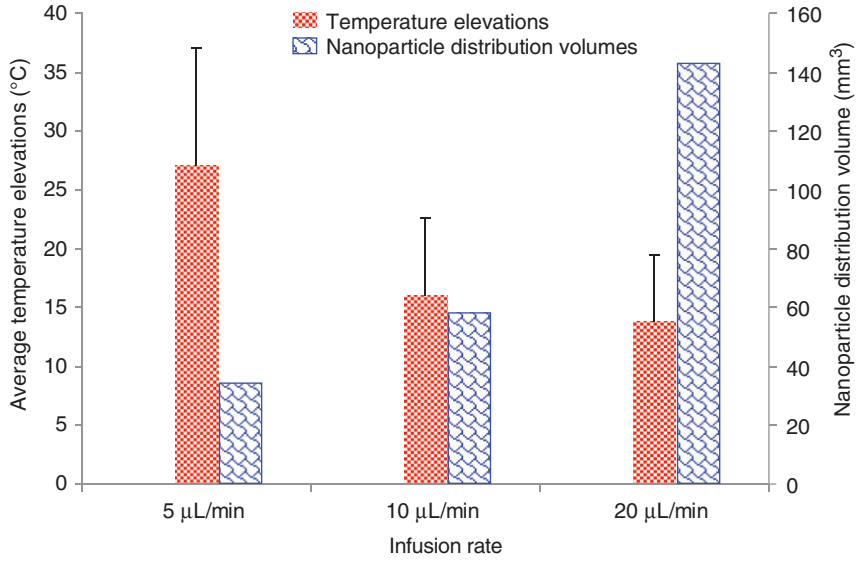

Figure 5. The effects of the ferrofluid infusion rate on both the average temperature elevations in the tumours and the calculated nanoparticle distribution volumes. The left bars represent the average temperature elevations in all tumours in individual groups, while the right bars are the calculated nanoparticle distribution volumes based on the constructed microCT scans.

average values of the temperature elevations in each group are illustrated in Figure 5. It is shown that 27°, 15°, and 14°C above the baseline temperature of 37°C are achieved for the infusion rate of 5, 10, and 20 μL/min, respectively. Although standard deviation in each group is high, there is a significant difference ($p < 0.05$) between the 5 μL/min group and any of the other two groups. Both Figures 4 and 5 illustrate that a smaller infusion flow rate would yield much higher temperature elevations in the tumour.

MicroCT images of nanoparticle distribution

Figure 6 gives a three-dimensional microCT image of a tumour containing nanoparticles. It is evident that the deposition of nanoparticles in tumours greatly increases the local pixel index number, which represents the average material density of the pixel volume. The tissue region containing nanoparticles appears bright, while the normal tumour region without nanoparticle is represented by dark colour. The variations of the pixel index number inside the nanoparticle region can be used to assess the nanoparticle concentration distribution, which typically is not uniform in the tumour. Using a single needle injection site in the tumour does not necessarily produce a perfectly regular shape of the nanoparticle distribution region. As shown in Figure 6, the shape is quite irregular, although the majority of the nanoparticles are confined to the injection site. It appears that nanoparticles transport through small cracks in the tumour and form those irregularly shaped branches.

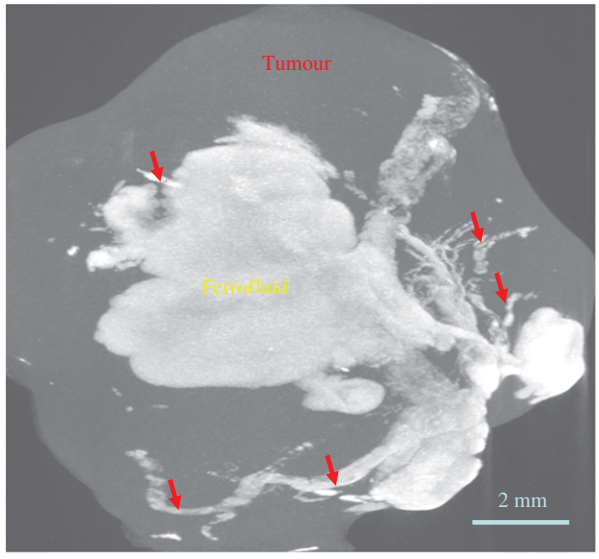

Figure 6. An obtained 3-D microCT scan image of a tumour with nanoparticle injection after the heating experiment. Red arrows represent ferrofluid filled cracks/voids within the tumour.

The observed temperature elevation variations among different ferrofluid infusion rate groups may be directly related to the nanoparticle distribution in the tumour, since the local nanoparticle concentration is proportional to the local SAR values. Using a pixel index number range of 55 and above, the total nanoparticle distribution volume can be calculated using the microCT analyses software. As shown in Figure 5, the nanoparticle distribution volumes are

Table 1. Nanoparticle distribution volume for different pixel number ranges.

	Nanoparticle distribution volume mm^3						
Pixel range	≥55*	55–60	60–65	65–70	70–75	75–80	80–85
Infusion without heating	36.52	17.51	8.48	3.17	1.20	0.70	0.30
Infusion + heating	40.57	20.52	7.13	2.20	1.21	1.09	0.69

*Pixel range of ≥55 represents the total nanoparticle distribution volume within the tumour.

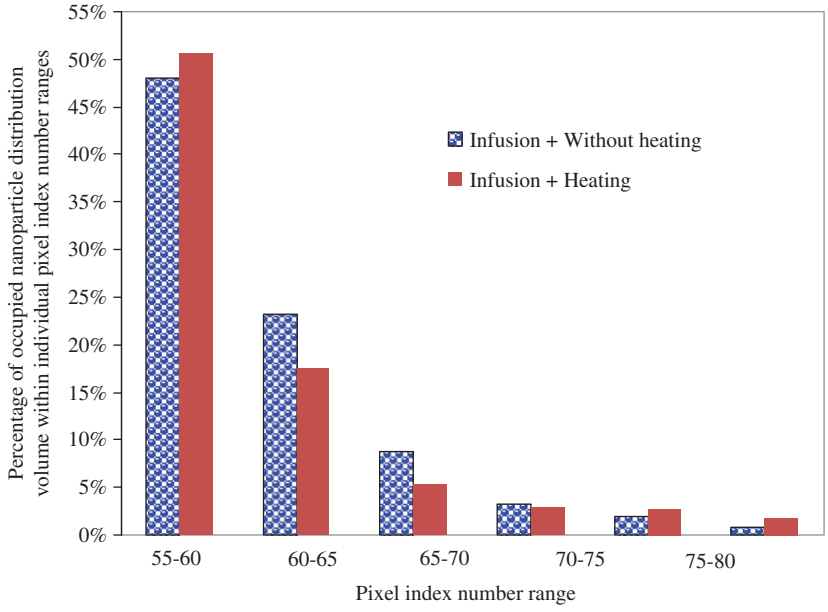

Figure 7. The percentages of occupied nanoparticle distribution volume within individual pixel index number ranges over the entire nanoparticle distribution volume, which is calculated using a threshold pixel index number of 55. The infusion flow rate of the ferrofluid is 5 μL/min.

36.52 ± 36.77, 57.71 ± 108.66, and $144.21 \pm 181.65\,mm^3$ for the infusion rate of 5, 10, and 20 μL/min, respectively. Decreasing the infusion rate confines the nanoparticles to a small distribution volume compared to that using larger infusion rates, this results in larger temperature elevations in the tumours.

In this study, we have selected various ranges of the pixel index number including 55–60, 60–65, 65–70, 70–75, 75–80, and 80–85. The range of 55–60 is associated with a low local nanoparticle concentration, while the range of 80–85 represents a high local nanoparticle concentration. Using different ranges, one can study the nanoparticle distribution volume associated with different nanoparticle concentrations. The results are presented in Table 1. The total overall nanoparticle distribution volume after infusion alone is $36.5\,mm^3$ (pixel number ≥ 55). Nanoparticles associated with a low local nanoparticle concentration (pixel index range of 55–60) occupy a total volume of $17.51\,mm^3$, while the volumes are decreasing with an increase in the nanoparticle concentration. Only $0.3\,mm^3$ pixel volumes are occupied by a high nanoparticle concentration (pixel index range of 80–85). Figure 7 illustrates the occupied nanoparticle distribution volume percentage for different pixel number ranges. Similar to Table 1, Figure 7 suggests that the distribution of the nanoparticles in the tumour is not uniform. The least concentrated nanoparticles represented by the pixel number range between 55 and 60 occupy almost half of the distribution volume ($17.5/36.5 = 48\%$). The percentage of the second range between 60 and 65 decreases more than half to 23%. A general pattern can be observed to suggest approximately 50% decrease from its previous range. If the different pixel index ranges represent individual nanoparticle concentrations, nanoparticles with lower local concentrations appear to occupy much bigger tissue volumes.

The nanoparticle distribution volumes have also been calculated based on scanning a group of

tumours after the heating experiment (the last row in Table 1 and red bars in Figure 7). Comparing the results of the heating group to the group without heating under the same ferrofluid infusion flow rate may offer insights on whether heating has induced any changes of nanoparticle distribution in tumours. Quantitative analyses of the nanoparticle distribution volumes of the two groups are illustrated in Table 1. At the infusion rate of 5 μL/min, the total nanoparticle distribution volume is approximately 36.5 mm^3 for the group without heating (pixel index number $\geq$ 55). The total nanoparticle distribution volume increases by 11%, to 40.6 mm^3 in the heating group. This suggests that overall the nanoparticles are dispersed in a larger tumour volume after heating. Figure 7 also shows that the percentage of the nanoparticle distribution volume associated with the lowest nanoparticle concentration (the 55–60 range) increases from approximately 48% in the group without heating to 51% in the heating group. Slight decreases in the percentages associated with higher nanoparticle concentrations are observed. Considering that the total infusion amount of the ferrofluid and the total numbers of nanoparticles are the same for both groups, and typically nanoparticle concentration varies from high in the tumour centre to low in the tumour periphery, one may interpret the increase in the nanoparticle distribution volume in the lower nanoparticle concentration range after heating as additional particle dispersion to the tumour periphery during the heating process.

Discussion

In hyperthermia treatment for killing cancer cells, maintaining sufficient temperature elevations for a period of time is essential for the treatment efficacy [24–28]. Typically, 43°C (6°C above 37°C) is the minimum temperature threshold to induce cytotoxic responses if the heating time is longer than 1 or 2 h. For higher temperature elevations, the required heating time can be dramatically decreased due to the inverse logarithmic relationship between temperature elevation and heating time. Previous experimental studies using animal models have demonstrated impressive tumour temperature above 60°C using various magnetic field strengths, nanoparticles, and nanoparticle concentrations [6, 8, 10–14]. The strength of the alternating magnetic field and the ferrofluid concentration are two important factors in magnetic nanoparticle hyperthermia to induce sufficient thermal dose to tumours. Previous investigations [18, 28] have shown that the volumetric heat generation rate or SAR is proportional to the square of the magnetic field strength H^2. A wide range of magnetic fields ranging from 3 to 25 kA/m were used in previous studies. In this study, one of our goals is to use a magnetic field strength in the lower limit to generate sufficient temperature elevations. The magnetic field strength has been increased from 2 kA/m in our previous study [16] to 3 kA/m in this study. In addition, the ferrofluid concentration increased almost 50% (5.8% versus 3.9%). So it is not a surprise to see in tumours with only 0.1 cm^3 ferrofluid injection much higher temperature elevations than in our previous study in muscle tissue [16]. An impressive average temperature elevation of 25°C above the normal body temperature was observed in the tumours with a slow infusion flow rate of 5 μL/min. A smaller amount of ferrofluid may be more clinically feasible and attractive to clinicians due to its shortened injection time, yet it still achieves sufficient temperature elevations such as 10°C to kill tumour cells.

Confining the same amount of nanoparticle solution to a smaller volume would result in a higher nanoparticle concentration in the centre of tumours. Based on previous theoretical derivations and experimental studies [7, 18, 29], the volumetric heat generation rate or SAR should be directly proportional to the nanoparticle concentration in the tumour. It is expected to see a correlation between temperature elevations and nanoparticle deposition distribution in tumours illustrated by the current study. The control parameter in the study is the ferrofluid infusion flow rate. Previous studies have shown that the infusion rate should be very small not to induce high local stress in tumour tissue. The maximal infusion rate used in this study is 20 μL/min, which did not create any micro-cracks in muscle tissue in our previous study [16]; however, the very irregular nanoparticle deposition patterns with many cracks shown by the microCT scans suggest that the prostatic tumours used in this study have a very low tolerance to elevated local pressure due to intratumoural injections. With a very small infusion rate of 5 μL/min, one can still see some crack formation in the tumours, although nanoparticles are more concentrated in the vicinity of the injection site. Formation of cracks in the tumour during intratumoural injections also makes repeatable and controlled nanoparticle distribution in the tumour difficult. Due to crack formation, more nanoparticles may be deposited in the tumour peripheral region rather than at the injection site. Our results have suggested that further lowering of the infusion rate may lead to fewer cracks and repeatable nanoparticle distribution patterns. As shown in the temperature elevation distributions, the standard deviation of the temperatures in the 5 μL/min group is much smaller than that of the other two groups with larger infusion rates. The measured temperature elevations in the 5 μL/min group are significantly higher than in the

other two groups, since the nanoparticles are more confined. One drawback of slow infusion rates is long infusion time, which may not be clinically feasible. Thus, more experimental studies are needed to use minimal ferrofluid amounts to achieve an acceptable injection time in clinical settings. This often requires more powerful magnetic fields to elevate the tumour temperature to similar levels, while using a small ferrofluid amount.

For this study, we are not certain whether the same amount resides in the tumour for the different injection rates. Previous experimental investigation by Johannsen et al. [23] has reported that 89.5% of the injected iron was detected in the tissue, while the remaining 10.5% may leak out or be carried away by the needle. One possible reason for the nanofluid leakage to the rest of the body may be due to large crack formation in tumours by the high pressure at the injection site, as shown in previous studies [30–32]. It is likely that a high infusion rate would result in big cracks, providing directing leakage channels to the rest of the mouse body. In this study, based on the observation that the tumour was self-contained in a sac, and trace of nanofluid (black colour) was not found in the surrounding mouse tissue, we speculate that limited dissemination of the nanofluid to the body occurred. Nevertheless, this is a limitation of our study. More experimental measurements are needed to quantify the leakage in the future.

The current study using high resolution microCT scans has demonstrated the capability of the imaging system to quantitatively assess nanoparticle distribution in tumours and how various parameters affect the distribution. The nanoparticle distribution volume has been used to analyse nanoparticles spreading in the tumours. Note that the distribution volume is a combination of all the pixel volumes containing sufficient nanoparticles to yield a measurable pixel index number above the baseline. Having a very small nanoparticle distribution volume has suggested that most of the nanoparticles are confined to a small region in the vicinity of the injection site. On the other hand, a big nanoparticle distribution volume is an indication of significant spreading to the tumour periphery. The smaller ferrofluid infusion rates result in more confined nanoparticle depositions, leading to a much higher temperature elevation at the tumour centre. When the particles are dispersed more towards the tumour periphery, it is expected to see smaller temperature elevations in the tumour. The measured temperature elevations affected by the ferrofluid infusion rate have demonstrated a correlation to the calculated nanoparticle distribution volumes.

Using different threshold pixel index numbers, one can extract the nanoparticle distribution volumes associated with various pixel index number ranges. Our study has shown that the nanoparticle distribution volumes for various pixel index number ranges are not uniform. The tumour volume having the smallest nanoparticle concentration (55–60 pixel index number range) occupies almost 50% of the nanoparticle distribution volume. The information can be very useful for theoretical simulations of temperature elevations in tumours, where an expression of the SAR distribution is needed. Analysing the nanoparticle distribution volumes at various concentration ranges may lead to better understanding of the nanoparticle concentration distribution in the tumour, and a relatively accurate SAR expression to model the heating pattern in magnetic nanoparticle hyperthermia.

Difference in the nanoparticle distribution volumes between a group of tumours without heating and another group after heating has illustrated possible effects of heating on the nanoparticle distribution. It has been shown that the nanoparticle distribution volume after heating is bigger than that without heating. This trend suggests re-distribution of nanoparticles during the heating. It has been well documented that hyperthermia can enhance vascular permeability in tumours to facilitate extravasation of nanostructures to tumour interstitial and further spreading to tumour periphery [20, 33–36]. The motion of nanoparticles in a porous medium is possible once the diffusion force overcomes other forces trapping them in their initial position. For example, nanoparticles, initially more confined to the injection site, may diffuse to the less concentrated region due to decrease in diffusion resistance by increased nanoparticle diffusivity due to cancer cell death in some tumour regions [36–37]. Another possibility of dispersing nanoparticles may be driven by the release of intracellular solution during heating. Local heating elevates tissue temperature, which in turn, may result in disruption of cell membrane. The originally bounded intracellular solution, once released, may elevate local pressure that induces convection of interstitial fluid and motion of nanoparticles. Although it was not directly visualised in most previous studies, our observation using microCT is consistent with a phenomenon known as the 'thermal bystander effect' [27]. Repeated heating has been used as a technique to kill tumour tissue completely in magnetic nanoparticle hyperthermia. Previous experimental studies [27] have shown a much more uniform temperature elevation in tumours in later repeated heating protocols using nanoparticles. This can be explained by a more dispersed nanoparticle distribution in the tumour after the initial heating. More quantitative microCT analyses, as well as multiscale theoretical modelling [38] are still needed to better understand the contributions of individual transport mechanisms to

the nanoparticle re-distribution in tumours during heating procedures.

In summary, temperature mapping in the implanted prostatic tumours during magnetic nanoparticle hyperthermia has illustrated the feasibility of elevating tumour temperatures higher than 50°C using very small amounts of ferrofluid injected in the tumour with a relatively low magnetic field. A high-resolution microCT imaging system is capable of visualising detailed nanoparticle concentration distribution in opaque tumours. The calculated nanoparticle distribution volume based on the microCT scans is useful to analyse nanoparticle deposition in the tumours. Slower ferrofluid infusion rates result in smaller nanoparticle distribution volumes in the tumours. Nanoparticles are more confined in the vicinity of the injection site with slower infusion rates, causing higher temperature elevations in the tumours. The increase in the nanoparticle distribution volume in the tumour group after the heating from that in the tumour group without heating suggests possible nanoparticle re-distribution in the tumours during the heating.

Declaration of interest: This research is supported in part by a National Science Foundation research grant CBET-0828728, a National Science Foundation MRI grant CBET-0821236, and a research grant from the UMBC Research Seed Fund Initiative. The research was performed in partial fulfilment of the requirements for the PhD degree from UMBC by Anilchandra Attaluri.

References

1. Truskey GA, Yuan F, Katz DF. Transport Phenomena in Biological Systems, second edn. Upper Saddle River, New Jersey: Prentice Hall; 2009.
2. National Cancer Institute. Available at http://www.cancer.gov/cancertopics/treatment/types-of-treatment.
3. Zhu L. Bioheat transfer. In: Kutz M, editor. Standard Handbook of Biomedical Engineering and Design, second edn. New York: McGraw-Hill; 2009.
4. Zhu L. Recent developments in biotransport. J Therm Sci Eng Appl 2010;2:040801 (1–11), http://asmedl.aip.org/getpdf/servlet/GetPDFServlet?filetype=pdf&id=JTSEBV000002000004@webtc.pdf&idtype=tocpdf.
5. Moroz P, Jones SK, Gray BN. Magnetically mediated hyperthermia: Current status and future directions. Int J Hyperthermia 2002;18:267–284.
6. Hergt R, Andra W, d'Ambly CG, Hilger I, Kaiser WA, Richter U, Schmidt H. Physical limits of hyperthermia using magnetite fine particles. IEEE T Magn 1998;34:3745–3754.
7. Rosensweig RE. Heating magnetic fluid with alternating magnetic field. J Magn Magn Mater 2002;252:370–374.
8. Jordan A, Scholz R, Wust P, Fahling H, Krause J, Wlodarczyk W, Sander B, Vogl T, Felix R. Effects of magnetic fluid hyperthermia (MFH) on C3H mammary carcinoma in vivo. Int J Hyperthermia 1997;13:587–605.
9. Jordan A, Wust P, Fahling H, John W, Hinz A, Felix R. Inductive heating of ferromagnetic articles and magnetic fluids: Physical evaluation of their potential for hyperthermia. Int J Hyperthermia 1993;9:51–68.
10. Johannsen M, Thiesen B, Gneveckow U, Taymoorian K, Waldofner N, Scholz R, Deger S, Jung K, Loening SA, Jordan A. Thermotherapy using magnetic nanoparticles combined with external radiation in an orthotropic rat model of prostate cancer. Prostate 2006;66:97–104.
11. Wust P, Gneveckow U, Johannsen M, Bohmer D, Henkel T, Kahmann F, Sehouli J, Felix R, Ricke J, Jordan A. Magnetic nanoparticles for interstitial thermotherapy – Feasibility, tolerance and achieved temperatures. Int J Hyperthermia 2006;22:673–685.
12. Hilger I, Hergt R, Kaiser WA. Towards breast cancer treatment by magnetic heating. J Magn Magn Mater 2005;293:314–319.
13. Du L, Zhou J, Wang X, Sheng L, Wang G, Xie X, Xu G, Zhao L, Liao Y, Tang J. Effect of local hyperthermia induced by nanometer magnetic fluid on the rabbit VX2 liver tumor model. Prog Nat Sci 2009;19:1705–1712.
14. Bruners P, Braunschweig T, Hodenius M, Pietsch H, Penzkofer T, Baumann M, Günther R, Schmitz-Rode T, Mahnken A. Thermoablation of malignant kidney tumors using magnetic nanoparticles: An in vivo feasibility study in a rabbit model. Cardio Vasc Intervent Radiol 2010;13:127–134.
15. Salloum M, Ma R, Weeks D, Zhu L. Controlling nanoparticle delivery in hyperthermia for cancer treatment: Experimental study in agarose gel. Int J Hyperthermia 2008a;24:337–345.
16. Salloum M, Ma R, Zhu L. An in-vivo experimental study of temperature elevations in animal tissue during magnetic nanoparticle hyperthermia. Int J Hyperthermia 2008b;24:589–601.
17. Salloum M, Ma R, Zhu L. Enhancement in treatment planning for magnetic nanoparticle hyperthermia: Optimization of the heat absorption pattern. Int J Hyperthermia 2009;25:309–321.
18. Attaluri AC, Ma R, Zhu L. Using microCT imaging technique to quantify heat generation distribution induced by magnetic nanoparticles for cancer treatments. J Heat Transfer 2011;133:011003–011008.
19. Berk DA, Yuan F, Leunig M, Jain R K. Fluorescence photobleaching with spatial fourier analysis: Measurement of diffusion in light-scattering media. Biophys J 1993;65:2428–2436.
20. Liu P, Zhang A, Xu Y, Xu L X. Study of non-uniform nanoparticle liposome extravasation in tumor. Int J Hyperthermia 2005;21:259–270.
21. Pluen A, Boucher Y, Ramanujan S, McKee TD, Gohongi R, DiTomaso E, Brown EB, Izumi Y, Campbell RB, Berk DA, Jain RK. Role of tumor-host interactions in interstitial diffusion of macromolecules: Cranial vs subcutaneous tumors. Proc Natl Acad Sci 2001;98:4628–4633.
22. Johannsen M, Thiesen B, Jordan A, Taymoorian K, Gneveckow U, Waldofner N, Scholz R, Koch M, Lein M, Jung K, Loening SA. Magnetic fluid hyperthermia (MFH) reduces prostate cancer growth in the orthotopic Dunning R3327 rat model. Prostate 2005;64:283–292.
23. Johannsen M, Gneveckow U, Thiesen B, Taymoorian K, Cho CH, Waldofner N, Scholz R, Jordan A, Loening SA, Wust P. Thermotherapy of prostate cancer using magnetic nanoparticles – Feasibility, imaging, and three-dimensional temperature distribution. Eur Urol 2007;52:1653–1661.
24. Engin K. Biological rationale for hyperthermia in cancer treatment (II). Neoplasma 1994;41:277–283.
25. Masuko Y, Tazawa K, Viroonchatapan E, Takemori S, Shimizu T, Fujimaki M, Nagae H, Sato H, Horikoshi I. Possibility of thermosensitive magnetoliposomes as a new

agent for electromagnetic induced hyperthermia. Biol Pharm Bull 1995;18:1802–1804.
26. Johannsen M, Jordan A, Scholz R, Koch M, Lein M, Deger S, Roigas J, Jung K, Loening S. Evaluation of magnetic fluid hyperthermia in a standard rat model of prostate cancer. J Endourol 2004;18:495–500.
27. Jordan A, Scholz R, Wust P, Fahling H, Felix R. Magnetic fluid hyperthermia (MFH): Cancer treatment with AC magnetic field induced excitation of biocompatible superparamagnetic nanoparticles. J Magn Magn Mater 1999;201:413–419.
28. Hergt R, Hiergeist R, Hilger I, Kaiser WA, Lapatnikov Y, Margel S, Richter U. Maghemite nanoparticles with very high AC-losses for application in RF-magnetic hyperthermia. J Magn Magn Mater 2004;270:345–357.
29. Hergt R, Andrä W. Magnetic hyperthermia and thermoablation. In: Andrä W and Nowakeds H, editors. Magnetism in Medicine: A Handbook, second edn. Weinheim, Germany: Wiley; 2007. pp 550–570.
30. McGuire S, Yuan F. Quantitative analysis of intratumoral infusion of color molecules. Am J Physiol Heart Circ Physiol 2001;281:H715–721.
31. Boucher Y, Brekken C, Netti PA, Baxter LT, Jain RK. Intratumoral infusion of fluid: Estimation of hydraulic conductivity and implications for the delivery of therapeutic agents. Br J Cancer 1998;78:1442–1448.
32. Wang Y, Wang H, Li CY, Yuan F. Effects of rate, volume, and dose of intratumoral infusion on virus dissemination in local gene delivery. Mol Cancer Ther 2006;5:362–366.
33. Ceelen WP, Hesse U, De Hemptinne B, Pattyn P. Hyperthermic intraperitoneal chemoperfusion in the treatment of locally advanced intra-abdominal cancer. Br J Surg 2000;87:1006–1015.
34. González-Moreno S, González-Bayón LA, Ortega-Pérez G. Hyperthermic intraperitoneal chemotherapy: Rationale and technique. World J Gastrointest Oncol 2010;2:68–75.
35. Ponce AM, Vujaskovic Z, Yuan F, Needham D, Dewhirst MW. Hyperthermia mediated liposomal drug delivery. Int J Hyperthermia 2006;22:205–213.
36. Zhang A, Mi X, Yang G, Xu LX. Numerical study of thermally targeted liposomal drug delivery in tumor. J Heat Transfer 2009;131:043209–043219.
37. Jang SH, Wientjes MG, Lu D, Au JL. Drug delivery and transport to solid tumors. Pharm Res 2003; 20:1337–1350.
38. Su D, Ma R, Salloum M, Zhu L. Multi-scale study of nanoparticle transport and deposition in tissues during an injection process. Med Biol Eng Comput 2010;48:853–863.